Caspase-mediated nuclear pore complex trimming in cell differentiation and endoplasmic reticulum stress

Ukrae H. Cho[1, *] and Martin W. Hetzer[1, *]

[1]Molecular and Cell Biology Laboratory, Salk Institute for Biological Studies, La Jolla, CA 92037, USA

*Correspondence should be addressed to
U.H.C (ucho@salk.edu) or M.W.H (hetzer@salk.edu)

Introductory Paragraph

During apoptosis, caspases degrade 7 out of ~30 nucleoporins (Nups) to irreversibly demolish the nuclear pore complex (NPC)[1,2]. However, for poorly understood reasons, caspases are also activated during differentiation at sublethal levels[3,4]. Here, we describe reversible, caspase-mediated NPC "trimming" during myogenesis. We find that sublethal levels of caspases selectively proteolyze 4 peripheral Nups, Nup358, Nup214, Nup153, and Tpr, resulting in the transient block of nuclear export pathways. Consequently, several nuclear export signal (NES)-containing focal adhesion proteins accumulate in the nucleus where they function as transcription cofactors[5]. One such protein, FAK (focal adhesion kinase), drives a global reconfiguration of MBD2 (methyl CpG binding domain protein 2)-mediated genome regulation. Caspase-mediated NPC trimming was also observed during neurogenesis and endoplasmic reticulum (ER) stress. Our results illustrate that NPC composition can be proteolytically modulated in response to non-apoptotic cues, and call for a reassessment of the death-centric view of caspases.

Caspase-mediated NPC proteolysis has been extensively studied in apoptotic cells[1,2], where it enables rapid nuclear translocation of pro-apoptotic proteins[6-9]. However, it remains unknown whether caspases target NPCs in differentiating cells where their activation is sublethal and transient. We therefore assessed Nup degradation in C2C12 cells undergoing myoblast-to-myotube transition[10]. Strikingly, during the first few days of myogenesis, 4 peripheral Nups, Nup358, Nup214, Nup153, and Tpr, were reversibly and completely degraded in a caspase-dependent manner (**Fig. 1a** and **Extended Data Fig. 1a**). Interestingly, Nup96 and Nup93, which form NPC scaffold and are cleaved by caspases during apoptosis[1], remained intact (**Fig. 1a**). This agrees with our previous report showing the persistence of the same Nup96 and Nup93 copies through the course of differentiation[11]. Hence, from the NPC quaternary structure perspective, caspases trim the cytoplasmic filaments and nuclear basket while sparing the membrane-traversing Nups, allowing rapid re-assembly of functional NPCs upon their quenching (**Fig. 1b**). Although calpains, another class of proteases that are activated during myogenesis[12], can proteolyze Nups like caspases[13], calpain inhibition delayed but did not prevent Nup degradation in differentiating C2C12 cells (**Extended Data Fig. 1a**).

To assess the functional consequences of NPC trimming, we examined the nuclear permeability barrier and active transport. The exclusion of ≥40-kDa dextrans demonstrates that the passive barrier remains functional (**Extended Data Fig. 1b**). This can be explained by the fact that none of the central FG Nups, such as Nup98 and Nup62, are targeted by caspases[1,2]. However, the removal of Nup358, Nup214, Nup153, or Tpr has been shown to block nuclear

35 export and cause nuclear accumulation of RNAs and NES-containing proteins[14-17]. We thus
36 monitored mRNA export by combining nuclear isolation and oligo(dT) bead-based poly(A)$^+$ RNA
37 purification. The nuclear-to-total mRNA ratio surges from 34% to 60% during differentiation,
38 indicating an impairment in nuclear export (**Fig. 1c**). Of note, the distribution of 18S rRNA and
39 *Gapdh* transcript remains unchanged (**Extended Data Fig. 1c**). The presence of RNAs with long
40 half-lives[18,19] allows cells to maintain homeostasis even when RNA export is temporarily inhibited.
41 We then asked if the localization of α-tubulin is affected. In control conditions, α-tubulin is
42 completely cytoplasmic due to multiple NESs[20]. Strikingly, one day after switching to
43 differentiation medium when NPCs are partially disintegrated, α-tubulin was detectable in the
44 nucleus, although at a relatively low level (**Fig. 1d**). We next checked if focal adhesion proteins
45 with genome-regulatory functions accumulate in the nucleus since they (1) contain NESs and (2)
46 are likely to be released to the cytoplasm by calpains in differentiating C2C12 cells[12] and enter
47 the nucleus by passive diffusion or by hitchhiking on their respective partner transcription factors[5].
48 Out of five focal adhesion proteins that we examined (**Supplementary Table 1**), four (Hic-5, zyxin,
49 paxillin, and FAK) transiently became nuclear during myogenesis (**Fig. 1e**). To confirm that the
50 nuclear accumulation of NES-containing focal adhesion proteins is a consequence of caspase-
51 mediated NPC trimming, we blocked Nup proteolysis using a pan-caspase inhibitor, Q-VD-OPh
52 (**Fig. 1f**). The nuclear entrapment of Hic-5, zyxin, paxillin, and FAK was notably suppressed, albeit
53 not fully. The residues can be ascribed to forced import by partner transcription factors (e.g.,
54 MBD2 for FAK[21] and nuclear receptors for Hic-5[22]). Finally, the cytoplasmic-to-nuclear ratio of
55 NES-GFP is significantly lower in myoblasts undergoing cell-cell fusion than in myotubes (1.26 vs
56 1.63; **Extended Data Fig. 2**). In short, differentiation-associated caspase activity blocks nuclear
57 export and leads to the nuclear retention of NES-containing proteins.
58 NPC proteolysis and its effect on nuclear transport were further analyzed by
59 immunofluorescence. Using four different antibodies (**Fig. 2a**), we first analyzed whether various
60 domains of Nup153 and Tpr are retained in late-stage apoptotic nuclei where caspase levels are
61 significantly higher than in differentiating cells. Surprisingly, only the C-terminal epitope of Tpr
62 dissociated from the NPC while proteolyzed Nup153 and Tpr N-terminus remained bound **(Fig.
63 2b)**. The nucleoplasmic pool of Crm1 was lost and it became confined to the nuclear periphery,
64 whereas the localization of importin-β was unaffected (**Extended Data Fig. 3a and b**).
65 Differentiating myoblasts exhibited an attenuated form of these phenotypes. The C-terminal
66 fragment of Tpr dissociated in 5-10% of the cells (**Fig. 2c and d**). This "TprC$^-$" population can be
67 clearly distinguished from dying cells by their nuclear morphology (**Extended Data Fig. 3c**).
68 Interestingly, even TprC$^-$ cells showed identical Crm1 localization to myoblasts in growth medium

69 (**Figure 2c**). This might explain why only a limited fraction of NES-containing proteins becomes
70 nuclear and the majority remain in the cytoplasm during NPC trimming (**Figure 1d and e**).
71 What determines whether a myoblast will be TprC^{-} or TprC^{+} during caspase activation?
72 During early apoptosis when caspase activity is modest, Tpr is cleaved likely at a single locus
73 within the Asp-rich region (**Fig. 2a**). As caspase levels increase, at least two additional aspartates
74 nearby are targeted for proteolysis[2]. Hence, TprC^{-} cells may represent a subpopulation that
75 experience highest-possible sublethal caspase activation in which Tpr is cleaved at multiple
76 aspartates and loses its C-terminus.
77 Among the focal adhesion proteins that accumulate in the nucleus, FAK is particularly
78 intriguing since it can facilitate cell survival, migration, cytoskeleton remodeling, and gene
79 (de)activation, all of which are required for cell differentiation[23]. For example, FAK binds and
80 removes MBD2, the main component of the gene-repressive NuRD (nucleosome remodeling and
81 deacetylation) complex[24], from methylated CpGs within the *Myog* promoter[21]. We speculated that
82 the FAK-mediated MBD2 dissociation during myotube formation is not limited to *Myog* but occurs
83 genome-wide. To test this, we employed CUT&RUN-sequencing[25] and examined how MBD2-
84 binding landscape changes in differentiating C2C12 cells (**Extended Data Fig. 4a**). In confluent
85 myoblasts, we detected 9791 MBD2-bound loci, and the number decreased to 354 in 24 hours
86 (**Fig. 3a**). Pharmacological caspase inhibition, which partially blocks the nuclear accumulation of
87 FAK (**Fig. 1f**), attenuates the loss of MBD2 binding (**Extended Data Fig. 4b**). Of note, MBD2
88 protein level remains constant during this time window, although it is eventually reduced in mature
89 myotubes (**Fig. 3b** and **Extended Data Fig. 4c**). After the completion of myogenic differentiation,
90 only few tens of MBD2-interacting sites were identifiable, suggesting that MBD2 binding rapidly
91 dissolves during myogenesis.
92 MBD2 overexpression has been reported to cause heterochromatin clustering like its
93 cousin, MeCP2 (methyl CpG-binding protein 2)[21,26]. However, we find that at the endogenous
94 levels, only MeCP2 localizes to the chromocenters and that MBD2 does not spatially overlap with
95 MeCP2 (**Extended Data Fig. 5a and b**), indicating that the two methyl CpG-binding proteins carry
96 out disparate tasks. To better understand MBD2 in the context of myogenesis, we further
97 analyzed MBD2 CUT&RUN-sequencing data from confluent myoblasts (Day 0 in **Fig. 3a**). About
98 a quarter of the peaks were in promoters, roughly one-third in introns, and another one-third in
99 distal intergenic regions (**Extended Data Fig. 6a**). Intense peaks were predominantly located
100 within promoters (**Extended Data Fig. 6b**), and the gene ontology (GO) term analysis revealed
101 that MBD2 primarily targets the promoter of the genes that have a direct link to myogenic
102 differentiation, with actin cytoskeleton organization (0030036) and muscle structure development

103 (0061061) genes being the top 2 categories (**Fig. 3c**, see **Extended Data Fig. 6c** for the GO
104 analysis of the entire MBD2-bound genes). *Mylpf* (myosin light chain, phosphorylatable, fast
105 skeletal muscle), whose mutation recently has been shown to cause a familial segmental
106 amyoplasia[27], is one noteworthy example (**Extended Data Fig. 6d**). In short, MBD2 binds cell
107 identity genes in muscle cells.

108 We then evaluated how transcription changes after MBD2 is removed from the promoters.
109 Considering that most MBD2-bound promoters are tri-methylated at Histone H3 lysine 4 in
110 myoblasts (**Extended Data Fig. 7a and b**), we expected that MBD2-target genes would be
111 upregulated after MBD2 dissociation, or the loss of the NuRD complex. However, RNA-
112 sequencing revealed that out of 1508 genes, only 218 exhibit >2-fold increase in transcript levels
113 whereas 336 show >2-fold decrease (**Fig. 3d** and **Extended Data Fig. 7c**). It is possible that
114 other gene-repressing mechanisms are taking over during myogenesis (e.g., non-MBD2 methyl
115 CpG binding proteins, heterochromatin reorganization, and gene-specific repressors).

116 To summarize, caspase-mediated NPC trimming coincides with nuclear sequestration of
117 NES-containing proteins (**Fig. 3e**), which can be transformative as in the case of FAK or
118 inconsequential (presumably) as in the case of α-tubulin. Our finding agrees with a previous
119 immunofluorescence-based study[28] that described (1) the transient nuclear translocation of an
120 NES-containing E3 ligase Nedd4 during myogenesis, which causes Pax7 degradation, and (2)
121 the 2- to 3-fold enhancement of myogenin activation in the presence of leptomycin b, a Crm1
122 inhibitor. We validated that a partial dose of leptomycin b increases myogenin at 24 hours-post-
123 differentiation by immunoblotting (**Extended Data Fig. 7d**).

124 We then sought to determine how caspase-3 is sublethally activated during myogenic
125 differentiation. Given the modest processing of caspase-9 (**Extended Data Fig. 8a**), we reasoned
126 that there might be additional factors that contribute to caspase-3 activation, and checked whether
127 caspase-inhibiting proteins are downregulated. Among eight inhibitors of apoptosis proteins
128 (IAPs), cIAP-1/2, XIAP, and survivin are considered the major caspase counteractors[29]. XIAP and
129 survivin can be regulated by the Notch signaling pathway[30,31], which plays a key role in
130 myogenesis. We thus monitored the expression of these IAPs during myotube formation in the
131 absence or presence of DAPT, a γ-secretase inhibitor that blocks Notch intracellular domain
132 release (**Fig. 4a**). We noted two intriguing points. First, survivin was dramatically downregulated
133 in the first 24 hours. Second, none of the examined IAP levels were affected by DAPT, indicating
134 that Notch signaling does not control these proteins during myogenesis.

135 To validate that survivin downregulation amplifies caspase-3 activity, we incubated
136 HCT116 cells with 1541B and/or YM155, chemicals that catalyze the proteolytic processing of

137 procaspase-3[32] or inhibits survivin transcription in cancer cells[33], respectively (**Extended Data**
138 **Fig. 8b**). 1541B gave rise to the active form of caspase-3 and induced the degradation of Tpr,
139 Nup153, and PARP (poly (ADP-ribose) polymerase) as well as cIAP-1 and XIAP[34,35], all of which
140 were accelerated/enhanced when 1541B was used in combination with YM155. (YM155 alone
141 decreases survivin, but not cIAP-1/2 and XIAP, and does not activate caspase-3.) This suggests
142 that survivin suppression potentiates caspase-3 activity.

143 We also discovered that calpain inhibition delays, but does not prevent, the activation of
144 caspase-3/12 and the degradation of peripheral Nups and PARP (**Extended Data Fig. 1a** and
145 **8c**). This signifies that, while calpains are upstream of caspases, there might be another caspase
146 activation pathway. Given that unfolded protein response is triggered in differentiating C2C12
147 cells[36], we surmise that procaspase-12 is processed by IRE1 and TRAF2 and converts
148 procaspase-3 to its active form as in ER stress conditions[37,38].

149 Next, we examined the relationship between caspase activation and myogenin, the main
150 driver of myogenesis (**Fig. 4b**). We generated a C2C12 stable cell line that expresses GFP-fused
151 myogenin in a doxycycline-dependent manner. Exogenous myogenin accelerated by a day the
152 upregulation of myosin heavy chain (MHC), and more importantly, the reduction of active
153 caspase-3, suggesting that a caspase-quenching pathway exists and is activated once myoblasts
154 pass a certain differentiation stage. Caspase inhibition prevented the expression of myogenin,
155 and thus MHC, as previously reported[10]. We then asked whether differentiation blockage by
156 caspase inhibition can be overridden by exogenous myogenin. Doxycycline-induced expression
157 of GFP-myogenin enabled the upregulation of both endogenous myogenin and MHC even when
158 a pan-caspase inhibitor was present. (The myotubes, however, appeared not as robust as the
159 ones formed in the presence of DMSO or doxycycline alone; data not shown). This demonstrates
160 that the key function of caspases is to upregulate myogenin, the master regulator, and that the
161 proteolyses of other targets are ancillary events that render cells amenable for differentiation.

162 We also explored whether caspase-3 activation is linked to the phosphatase activity of
163 calcineurin (**Fig. 4c**), as it is required for the nuclear translocation of NFAT (nuclear factor of
164 activated T-cells) and the transcriptional activation of myogenin[39]. We differentiated C2C12 cells
165 in the absence or presence of FK506, a calcineurin-inhibiting macrolide, and found that the p17
166 form of caspase-3 arises even when myogenin upregulation is blocked. This result illustrates that
167 the calcineurin/NFAT/myogenin pathway is orthogonal to the caspase/myogenin pathway. Taken
168 together, we have identified a new cascade – (1) caspase activation, (2) peripheral Nup
169 degradation, and (3) nuclear retention of NES-containing proteins – that regulates the expression
170 of myogenin[24], Pax7[28], and other myogenesis-related genes (**Fig. 4d**). Our model predicts that,

171 at the individual cell level, NPC trimming will precede and coincide briefly with myogenin
172 expression. Consistently, we could identify both myogenin-negative and -positive TprC^{-} C2C12
173 cells (**Fig. 4e**). The same transitory cell states appear in differentiating primary myoblasts as well
174 (**Extended Data Fig. 9**). Lastly, we found that pharmacological ERK1/2 inhibition, which recently
175 has been shown to stimulate myogenesis[40], accelerates survivin downregulation, caspase-3
176 activation, Nup153 degradation, and myogenin induction (**Extended Data Fig. 8d**). This highlights
177 that caspase-mediated NPC trimming is one of the earliest key events in myogenesis.

178 We then asked whether caspase-mediated NPC trimming is a general phenomenon
179 associated with cell differentiation. Neural precursor cells were differentiated into mature, post-
180 mitotic neurons, and caspase-related events were analyzed (**Fig. 5a**). As in myogenic
181 differentiation, survivin is highly expressed in precursor cells but undetectable in mature neurons.
182 As survivin decreases, caspase-3 is activated and Nup153 and PARP are degraded. This
183 suggests that caspases play similar roles during neuronal differentiation, albeit over a longer
184 duration.

185 We also tested whether partial NPC disintegration takes place during ER stress since the
186 calpain/caspase activation pathway in unfolded protein response is similar to that in myogenesis.
187 C2C12 myotubes, reserve cells, and myoblasts were treated with 1 μg/mL tunicamycin (**Fig. 5b**).
188 Active caspase-3 arose in all three cell types and Tpr and Nup153 degradation was recognizable
189 by 18 hours in C2C12 myoblasts and reserve cells; however, in myotubes, the two Nups were
190 fully proteolyzed by 6 hours. The result can be attributed to the difference in survivin and XIAP
191 expression levels, both of which are lowest in myotubes at 0 hour. We conclude that NPC trimming
192 occurs during ER stress at varying rates in different cell types. ER stress-induced NPC trimming
193 exhibits multiple similarities to that during myogenesis: (1) the average cytoplasmic-to-nuclear
194 ratio of NES-GFP of myonuclei decreased from 1.60 to 1.44 (**Extended Data Fig. 10a**), (2) 5-10%
195 of myotubes become TprC^{-} (**Extended Data Fig. 10b**), and (3) Nup93 remains unaffected,
196 suggesting that scaffold Nups are protected from caspases compared to peripheral Nups (**Fig.
197 5b**). Additionally, we tested whether low-level but sustained ER stress induces the same
198 phenotype in myotubes (**Fig. 5c**). In fact, several myopathies involve chronic, rather than acute,
199 ER stress and caspase activation[41]. We maintained differentiated C2C12 cells at low doses of
200 tunicamycin (<50 ng/mL) for a week, and again, major peripheral Nups were noticeably degraded
201 while the breakdown of Nup93 was minimal. NPC trimming may contribute to cellular homeostasis
202 loss in muscular diseases that accompany ER stress (**Fig. 5d**).

203 In summary, our study demonstrates that the NPC cytoplasmic filaments and nuclear
204 basket are transiently removed by caspases in differentiating and ER-stressed cells. This process

205 is distinct from terminal NPC destruction in apoptosis. Caspase-mediated NPC trimming is a
206 reversible process that, for a set period during differentiation, impairs nuclear export. We found
207 that during myogenesis, it is exploited to increase the nuclear levels of focal adhesion proteins
208 that can double as transcription cofactors. In addition, NPC trimming could reset NPC-genome
209 interaction during differentiation. NPCs bind and regulate cell identity genes[42], and transient
210 proteolysis of the nuclear basket can be an elegant reinitialization mechanism. During ER stress,
211 the same phenomenon can potentially be utilized to curtail mRNA export, thereby reducing the
212 protein synthesis/folding load in the ER. We primarily focused on the NPC, but the degradation of
213 other caspase substrates might promote cell differentiation in their own ways. For example,
214 caspases target several cytoskeletal proteins (e.g. αII-spectrin in **Fig. 1a**) and can accelerate
215 morphological transformation. Proteolytic inactivation of transcription factors[43,44] and translation-
216 related proteins can also facilitate transcriptome and proteome turnover. Our findings support the
217 idea that caspases initially evolved to change cell morphology, behavior, and identity, and that
218 apoptosis is rather an extreme form of caspase-mediated cellular transformation[3,4].

Acknowledgments

We thank the members of the Hetzer lab and Jongmin Kim (Massachusetts General Hospital) for the critical reading of the manuscript; Kenneth Diffenderfer and Aimee Pankonin (Stem Cell Core Facility at the Salk Institute) for help with neurogenesis; Carol Marchetto and Fred Gage (the Salk Institute) for providing H9 embryonic stem cells; Lorenzo Puri, Alexandra Sacco, and Luca Caputo (Sanford Burnham Prebys) for helpful discussions and sharing mouse primary myoblasts. This work was supported by a Glenn Foundation for Medical Research Postdoctoral Fellowship in Aging Research (U.H.C.), the NOMIS foundation (M.W.H), and the National Institutes of Health (R01 NS096786 to M.W.H.).

Author contributions

U.H.C. performed experiments. U.H.C. and M.W.H. conceived the study and wrote the manuscript.

Data availability statement

CUT&RUN- and RNA-sequencing data have been uploaded to the Gene Expression Omnibus (GEO) database (NCBI) under accession numbers GSE183520 and GSE183521.

Competing financial interests

The authors declare no competing financial interests.

References

1 Patre, M. *et al.* Caspases target only two architectural components within the core structure of the nuclear pore complex. *J Biol Chem* **281**, 1296-1304 (2006).

2 Ferrando-May, E. *et al.* Caspases mediate nucleoporin cleavage, but not early redistribution of nuclear transport factors and modulation of nuclear permeability in apoptosis. *Cell Death Differ* **8**, 495-505 (2001).

3 Connolly, P. F., Jager, R. & Fearnhead, H. O. New roles for old enzymes: killer caspases as the engine of cell behavior changes. *Front Physiol* **5**, 149 (2014).

4 Burgon, P. G. & Megeney, L. A. Caspase signaling, a conserved inductive cue for metazoan cell differentiation. *Semin Cell Dev Biol* **82**, 96-104 (2018).

5 Hervy, M., Hoffman, L. & Beckerle, M. C. From the membrane to the nucleus and back again: bifunctional focal adhesion proteins. *Curr Opin Cell Biol* **18**, 524-532 (2006).

6 Diaz-Moreno, I., Velazquez-Cruz, A., Curran-French, S., Diaz-Quintana, A. & De la Rosa, M. A. Nuclear cytochrome c - a mitochondrial visitor regulating damaged chromatin dynamics. *FEBS Lett* **592**, 172-178 (2018).

7 Bano, D. & Prehn, J. H. M. Apoptosis-Inducing Factor (AIF) in Physiology and Disease: The Tale of a Repented Natural Born Killer. *EBioMedicine* **30**, 29-37 (2018).

8 Kamada, S., Kikkawa, U., Tsujimoto, Y. & Hunter, T. Nuclear translocation of caspase-3 is dependent on its proteolytic activation and recognition of a substrate-like protein(s). *J Biol Chem* **280**, 857-860 (2005).

9 Wang, Y. *et al.* A nuclease that mediates cell death induced by DNA damage and poly(ADP-ribose) polymerase-1. *Science* **354**, aad6872 (2016).

10 Fernando, P., Kelly, J. F., Balazsi, K., Slack, R. S. & Megeney, L. A. Caspase 3 activity is required for skeletal muscle differentiation. *Proc Natl Acad Sci U S A* **99**, 11025-11030 (2002).

11 Toyama, B. H. *et al.* Visualization of long-lived proteins reveals age mosaicism within nuclei of postmitotic cells. *J Cell Biol* **218**, 433-444 (2019).

266 12 Louis, M., Zanou, N., Van Schoor, M. & Gailly, P. TRPC1 regulates skeletal myoblast
267 migration and differentiation. *J Cell Sci* **121**, 3951-3959 (2008).

268 13 Bano, D. *et al.* Alteration of the nuclear pore complex in Ca(2+)-mediated cell death. *Cell*
269 *Death Differ* **17**, 119-133 (2010).

270 14 Hutten, S. & Kehlenbach, R. H. Nup214 is required for CRM1-dependent nuclear protein
271 export in vivo. *Mol Cell Biol* **26**, 6772-6785 (2006).

272 15 Ullman, K. S., Shah, S., Powers, M. A. & Forbes, D. J. The nucleoporin nup153 plays a critical
273 role in multiple types of nuclear export. *Mol Biol Cell* **10**, 649-664 (1999).

274 16 Aksenova, V. *et al.* Nucleoporin TPR is an integral component of the TREX-2 mRNA export
275 pathway. *Nat Commun* **11**, 4577 (2020).

276 17 Forler, D. *et al.* RanBP2/Nup358 provides a major binding site for NXF1-p15 dimers at the
277 nuclear pore complex and functions in nuclear mRNA export. *Mol Cell Biol* **24**, 1155-1167
278 (2004).

279 18 Yi, X., Tesmer, V. M., Savre-Train, I., Shay, J. W. & Wright, W. E. Both transcriptional and
280 posttranscriptional mechanisms regulate human telomerase template RNA levels. *Mol Cell*
281 *Biol* **19**, 3989-3997 (1999).

282 19 Lee, J. E., Lee, J. Y., Wilusz, J., Tian, B. & Wilusz, C. J. Systematic analysis of cis-elements
283 in unstable mRNAs demonstrates that CUGBP1 is a key regulator of mRNA decay in muscle
284 cells. *PLoS One* **5**, e11201 (2010).

285 20 Schwarzerova, K. *et al.* Tubulin is actively exported from the nucleus through the
286 Exportin1/CRM1 pathway. *Sci Rep* **9**, 5725 (2019).

287 21 Luo, S. W. *et al.* Regulation of heterochromatin remodelling and myogenin expression during
288 muscle differentiation by FAK interaction with MBD2. *EMBO J* **28**, 2568-2582 (2009).

289 22 Alpha, K. M., Xu, W. & Turner, C. E. Paxillin family of focal adhesion adaptor proteins and
290 regulation of cancer cell invasion. *Int Rev Cell Mol Biol* **355**, 1-52 (2020).

291 23 Kleinschmidt, E. G. & Schlaepfer, D. D. Focal adhesion kinase signaling in unexpected places.
292 *Curr Opin Cell Biol* **45**, 24-30 (2017).

293 24 Wood, K. H. & Zhou, Z. Emerging Molecular and Biological Functions of MBD2, a Reader of
294 DNA Methylation. *Front Genet* **7**, 93 (2016).

295 25 Skene, P. J. & Henikoff, S. An efficient targeted nuclease strategy for high-resolution mapping
296 of DNA binding sites. *eLife* **6** (2017).

297 26 Brero, A. *et al.* Methyl CpG-binding proteins induce large-scale chromatin reorganization
298 during terminal differentiation. *J Cell Biol* **169**, 733-743 (2005).

299 27 Chong, J. X. *et al.* Mutations in *MYLPF* Cause a Novel Segmental Amyoplasia that Manifests
300 as Distal Arthrogryposis. *Am J Hum Genet* **107**, 293-310 (2020).

301 28 Bustos, F. *et al.* NEDD4 Regulates PAX7 Levels Promoting Activation of the Differentiation
302 Program in Skeletal Muscle Precursors. *Stem Cells* **33**, 3138-3151 (2015).

303 29 Srinivasula, S. M. & Ashwell, J. D. IAPs: what's in a name? *Mol Cell* **30**, 123-135 (2008).

304 30 Lee, C. W., Raskett, C. M., Prudovsky, I. & Altieri, D. C. Molecular dependence of estrogen
305 receptor-negative breast cancer on a notch-survivin signaling axis. *Cancer Res* **68**, 5273-5281
306 (2008).

307 31 Liu, W. H., Hsiao, H. W., Tsou, W. I. & Lai, M. Z. Notch inhibits apoptosis by direct interference
308 with XIAP ubiquitination and degradation. *EMBO J* **26**, 1660-1669 (2007).

309 32 Wolan, D. W., Zorn, J. A., Gray, D. C. & Wells, J. A. Small-molecule activators of a proenzyme.
310 *Science* **326**, 853-858 (2009).

311 33 Nakahara, T. *et al.* YM155, a novel small-molecule survivin suppressant, induces regression
312 of established human hormone-refractory prostate tumor xenografts. *Cancer Res* **67**, 8014-
313 8021 (2007).

314 34 Guicciardi, M. E. *et al.* Cellular inhibitor of apoptosis 1 (cIAP-1) degradation by caspase 8
315 during TNF-related apoptosis-inducing ligand (TRAIL)-induced apoptosis. *Exp Cell Res* **317**,
316 107-116 (2011).

317 35 Hornle, M. *et al.* Caspase-3 cleaves XIAP in a positive feedback loop to sensitize melanoma
318 cells to TRAIL-induced apoptosis. *Oncogene* **30**, 575-587 (2011).

319 36 Nakanishi, K., Sudo, T. & Morishima, N. Endoplasmic reticulum stress signaling transmitted
320 by ATF6 mediates apoptosis during muscle development. *J Cell Biol* **169**, 555-560 (2005).

321 37 Morishima, N., Nakanishi, K., Takenouchi, H., Shibata, T. & Yasuhiko, Y. An endoplasmic
322 reticulum stress-specific caspase cascade in apoptosis. Cytochrome c-independent activation
323 of caspase-9 by caspase-12. *J Biol Chem* **277**, 34287-34294 (2002).

324 38 Yoneda, T. *et al.* Activation of caspase-12, an endoplastic reticulum (ER) resident caspase,
325 through tumor necrosis factor receptor-associated factor 2-dependent mechanism in
326 response to the ER stress. *J Biol Chem* **276**, 13935-13940 (2001).

327 39 Armand, A. S. *et al.* Cooperative synergy between NFAT and MyoD regulates myogenin
328 expression and myogenesis. *J Biol Chem* **283**, 29004-29010 (2008).

329 40 Eigler, T. *et al.* ERK1/2 inhibition promotes robust myotube growth via CaMKII activation
330 resulting in myoblast-to-myotube fusion. *Dev Cell* **56**, 3349-3363 e3346 (2021).

331 41 Afroze, D. & Kumar, A. ER stress in skeletal muscle remodeling and myopathies. *FEBS J* **286**,
332 379-398 (2019).

333 42 Cho, U. H. & Hetzer, M. W. Nuclear Periphery Takes Center Stage: The Role of Nuclear Pore
334 Complexes in Cell Identity and Aging. *Neuron* **106**, 899-911 (2020).

335 43 Dick, S. A. *et al.* Caspase 3 cleavage of Pax7 inhibits self-renewal of satellite cells. *Proc Natl*
336 *Acad Sci U S A* **112**, E5246-5252 (2015).

337 44 Bell, R. A. V. *et al.* Chromatin reorganization during myoblast differentiation involves the
338 caspase-dependent removal of SATB2. *bioRxiv* (2019).
339

Fig. 1 | Caspases proteolyze peripheral Nups during myogenesis (+ **Extended Data Fig. 1-2**)

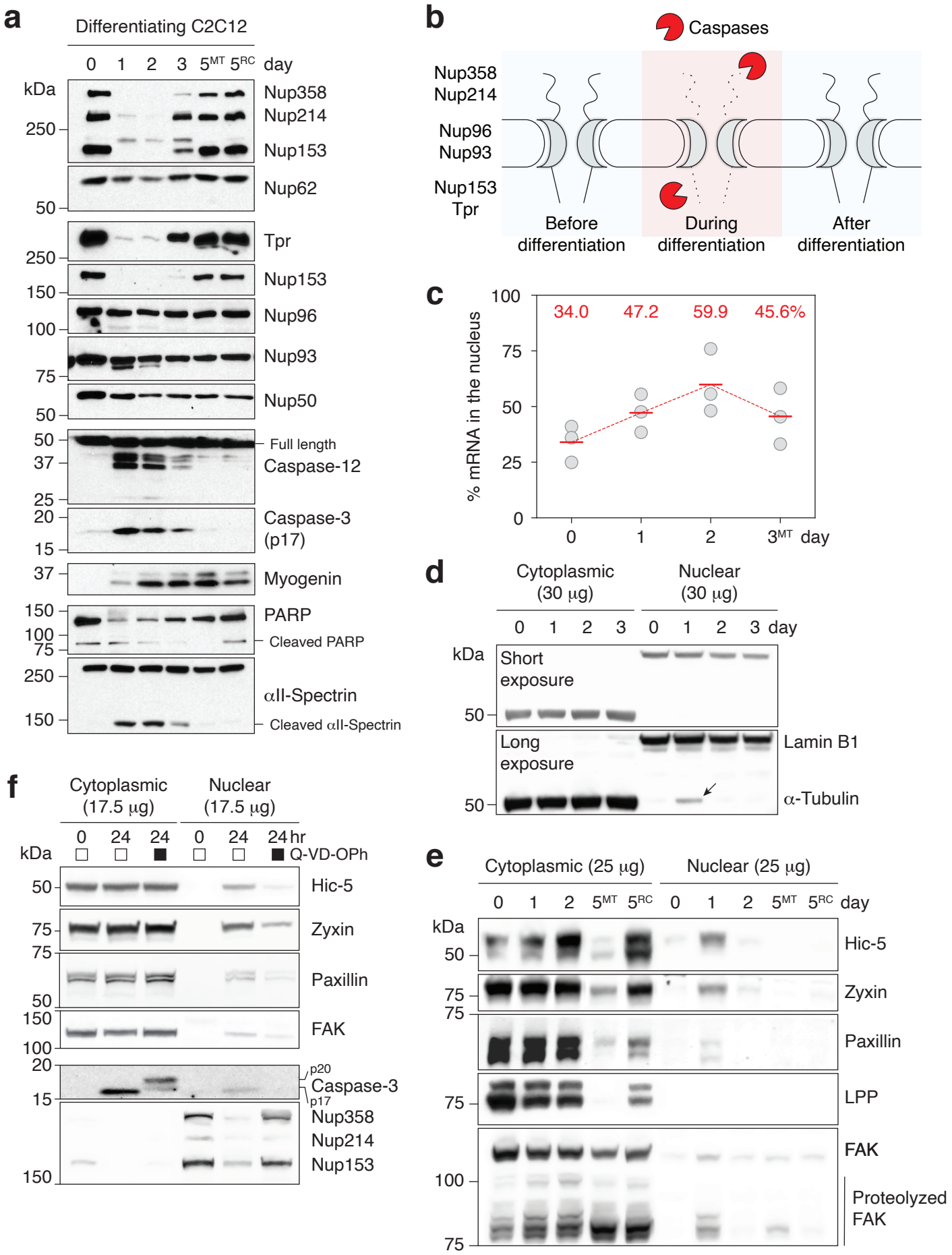

Fig. 2 | Tpr C-terminal fragment dissociates from the NPC during myogenesis (+ **Extended Data Fig. 3**)

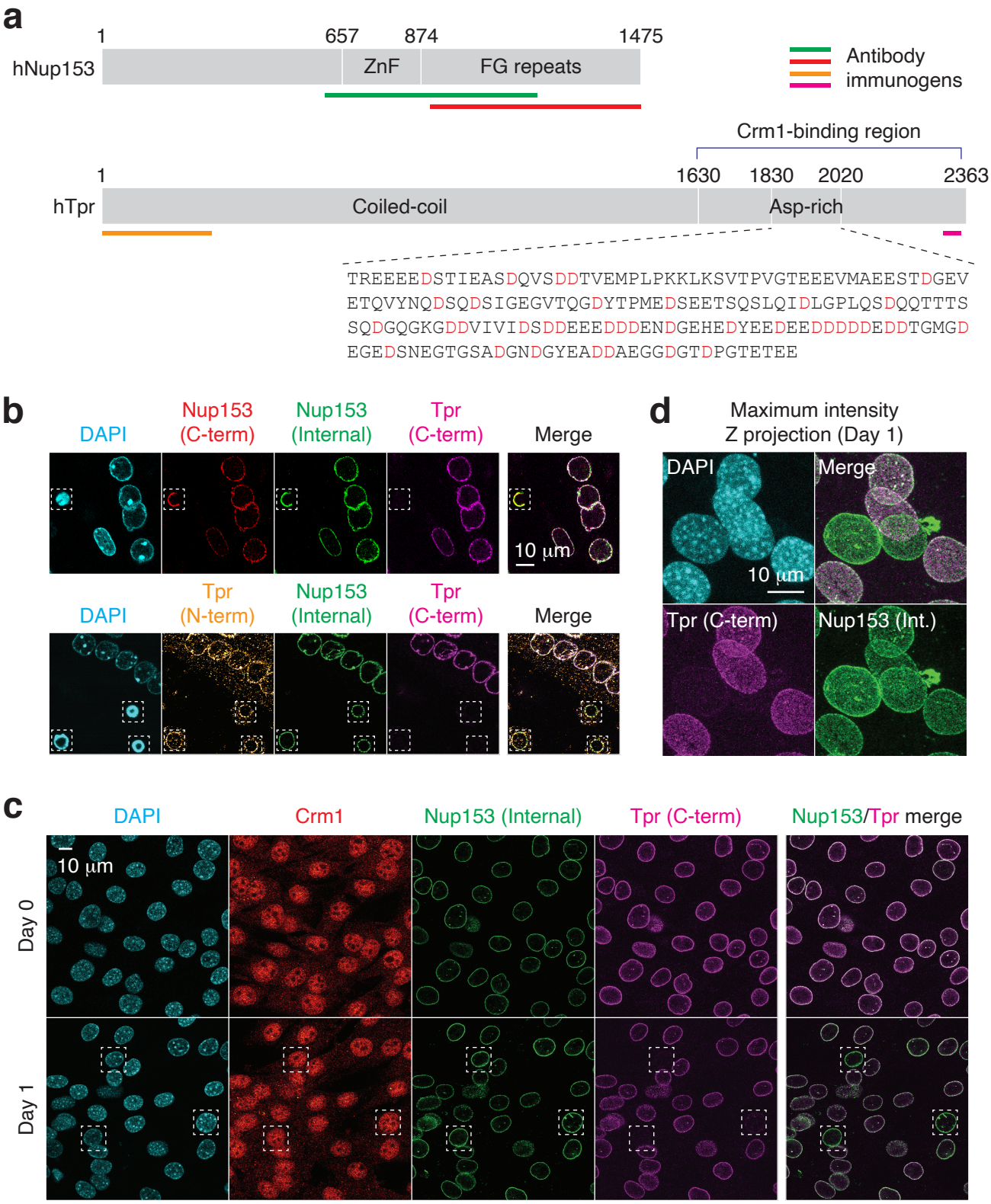

Fig. 3 | Transient nuclear retention of FAK resets MBD2-mediated genome regulation during myogenesis (+ **Extended Data Fig. 4-7**)

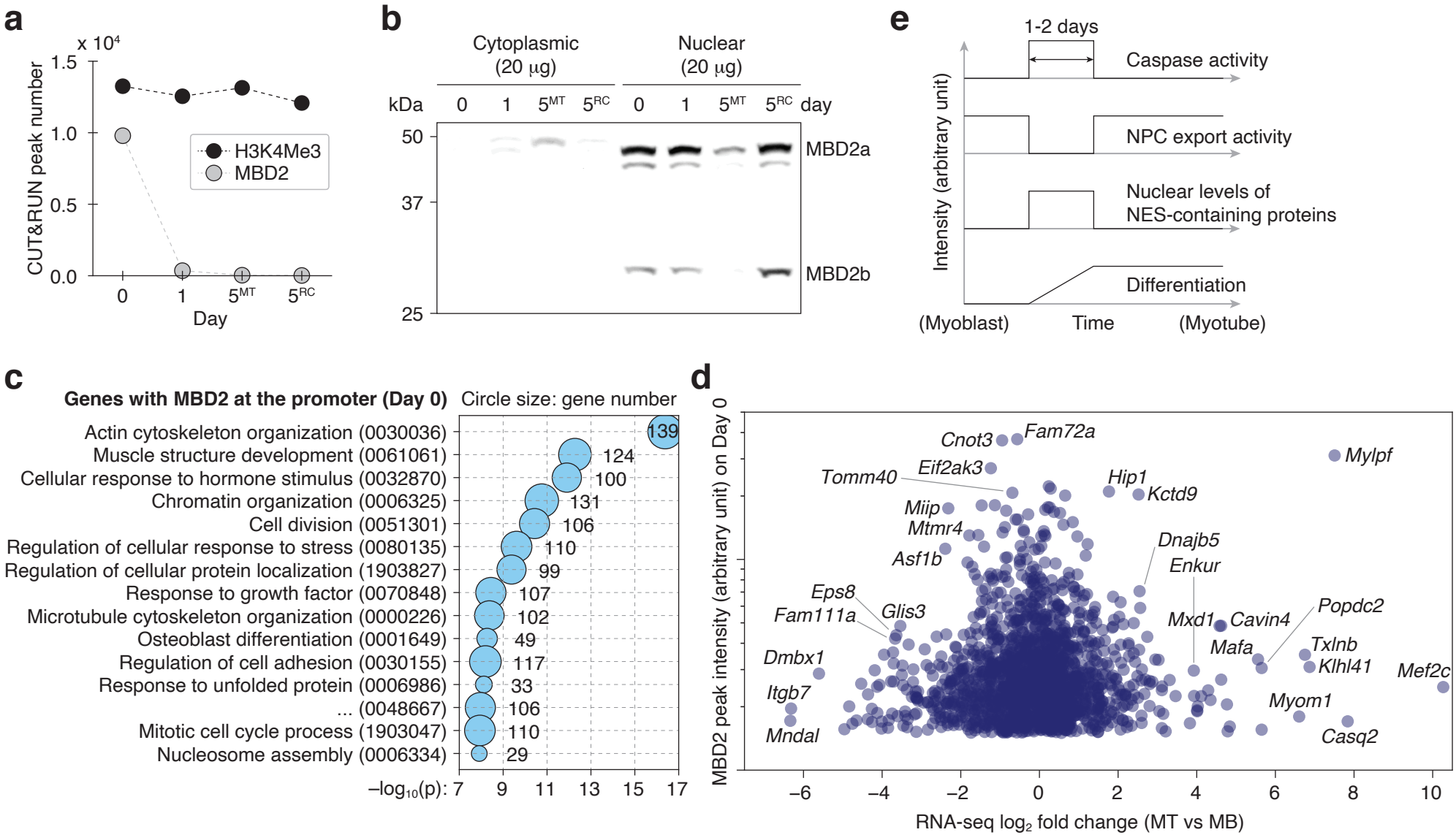

Fig. 4 | Caspase activation integrates multiple pathways for myogenin upregulation (+ **Extended Data Fig. 8-9**)

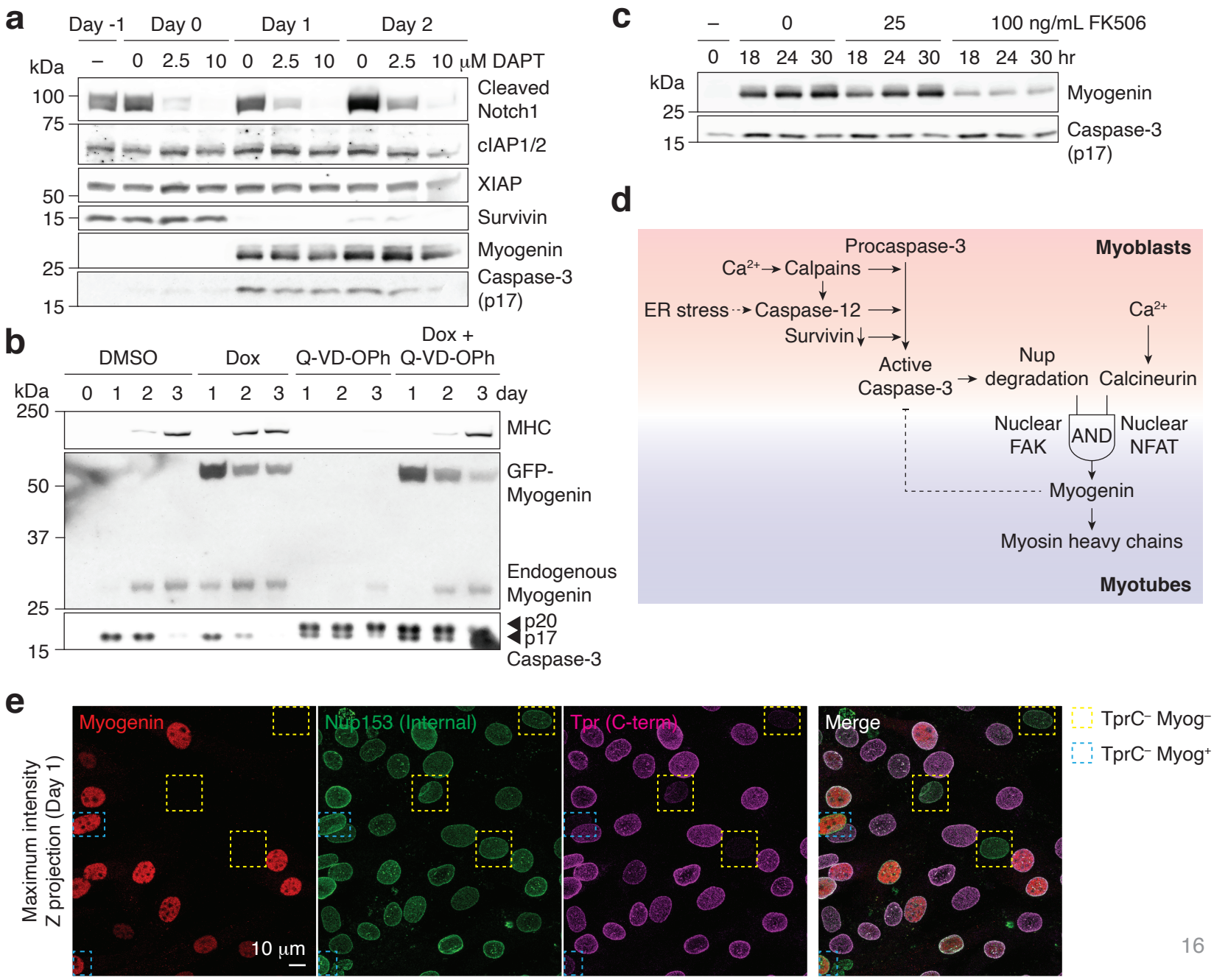

Fig. 5 | Caspase-mediated NPC trimming occurs during neurogenesis and ER stress (+ **Extended Data Fig. 10**)

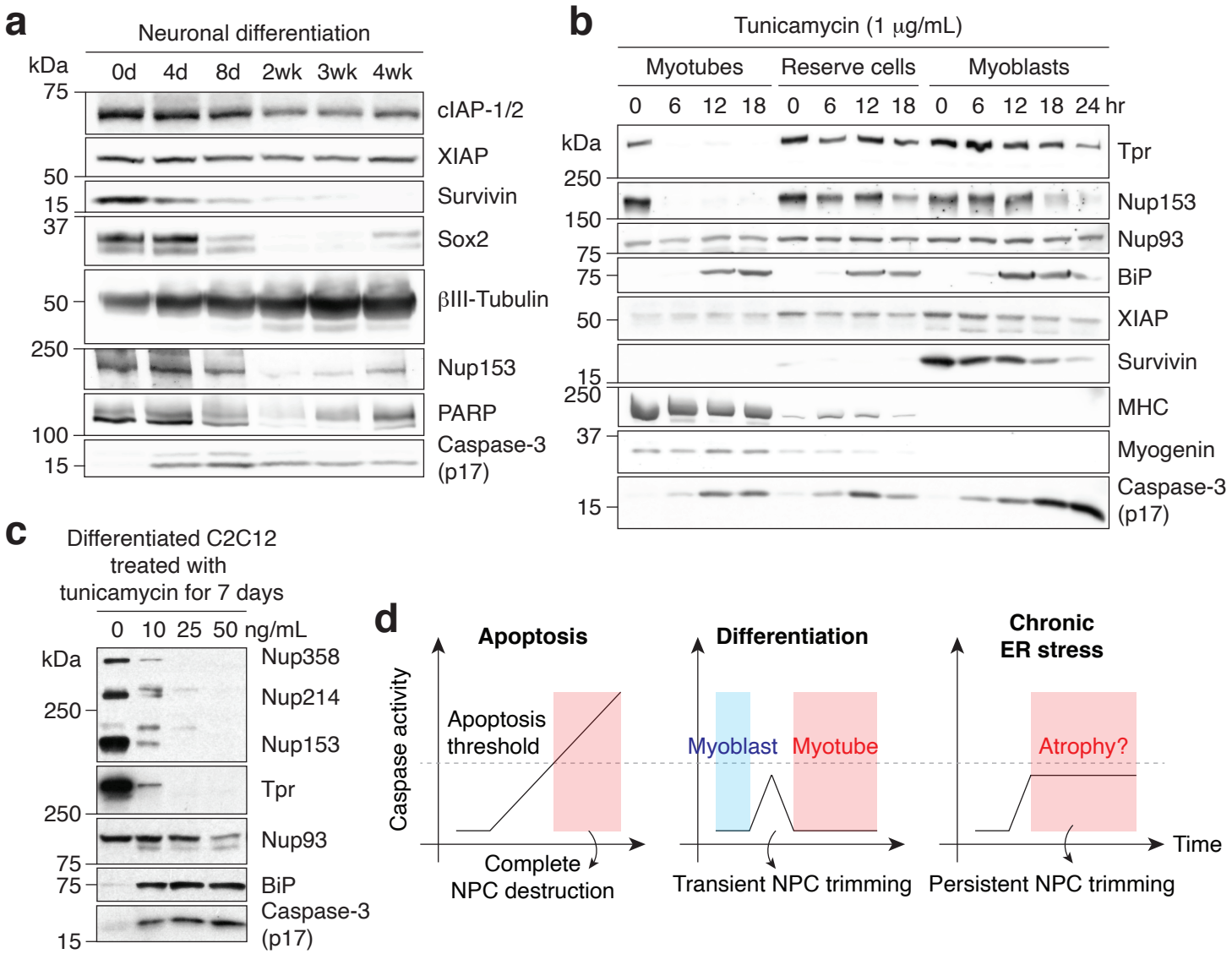

Figure Legends

Figure 1 | Caspases proteolyze peripheral Nups during myogenesis. a, Immunoblots showing the degradation of Nups, PARP, and αII-spectrin, the proteolytic activation of caspase-3 and -12, and the upregulation of myogenin in differentiating C2C12. MT: myotubes, RC: reserve cells. **b,** Schematic representation of caspase-mediated NPC trimming during myogenic differentiation. **c,** Nuclear-to-total mRNA ratio in C2C12 cells undergoing myoblast-to-myotube transition. In red is the average value of three replicates from each point. **d,** Localization of lamin B1 and α-tubulin in differentiating C2C12 cells was assessed by immunoblotting. Nuclear α-tubulin is marked with an arrow. 30 μg of protein from cytoplasmic or nuclear lysate was loaded to each lane. **e,** Cytoplasmic and nuclear levels of NES-containing focal adhesion proteins in differentiating C2C12 cells were assessed by immunoblotting. For both cytoplasmic and nuclear fractions, 25 μg of protein was loaded per lane. **f,** C2C12 cells were differentiated in the absence or presence of a pan-caspase inhibitor, Q-VD-OPh (30 μM) for 24 hours, and nuclear and cytoplasmic fractions were obtained. Nuclear accumulation of NES-containing focal adhesion proteins, caspase-mediated NPC trimming, and p53 degradation were examined by western blotting. 17.5 μg of cytoplasmic or nuclear protein was loaded per lane.

Figure 2 | Tpr C-terminal fragment dissociates from the NPC during myogenesis. a, Domain architecture of human Nup153 and Tpr. Immunogenic fragments used to generate Nup153 and Tpr antibodies are mapped on each protein. Aspartates (D) in Tpr aspartate-rich region are colored in red. **b,** C2C12 cells were immunostained using two Nup153 and two Tpr antibodies. See **a** for corresponding immunogenic regions. In dashed boxes are apoptotic nuclei. **c,** C2C12 cells undergoing myogenic differentiation (day 0 and 1) were immunostained for Crm1, Nup153, and Tpr. In dashed boxes are $TprC^{-}$ cells. **d,** $TprC^{-}$ cells were identified by immunofluorescence and maximum intensity Z projection micrographs were reconstructed from confocal imaging.

Figure 3 | Transient nuclear retention of FAK resets MBD2-mediated genome regulation during myogenesis. a, The number of MBD2 and H3K4Me3 CUT&RUN peaks in differentiating C2C12 cells. **b,** Cytoplasmic and nuclear levels of MBD2 in differentiating C2C12 cells were determined by western blotting. 20 μg of protein was loaded per lane. **c,** GO analysis of the genes whose promoters are bound with MBD2 in confluent myoblasts (day 0). In parentheses are seven-digit GO IDs. GO ID 0048667 corresponds to “cell morphogenesis involved in neuron differentiation”. **d,** Transcriptional changes after MBD2 is removed from the promoter of respective

genes. Y-axis denotes MBD2 CUT&RUN peak intensity in confluent myoblasts (day 0). **e,** Schematic representation of caspase activation and downstream events that take place during myogenesis.

Figure 4 | Caspase activation integrates multiple pathways for myogenin upregulation. a, Immunoblots showing the expression levels of cleaved Notch1, caspase-inhibiting proteins (cIAP1/2, XIAP, and survivin), myogenin, and active caspase-3 (p17) in C2C12 cells. DAPT was added at 0, 2.5, or 10 μM on day -1, and maintained throughout differentiation. **b,** C2C12 stable cell line that expresses GFP-myogenin in a doxycycline-dependent manner was differentiated in the absence or presence of 0.5 μM doxycycline and/or 30 μM Q-VD-OPh. Myosin heavy chain (MHC), exogenous and endogenous myogenin, and caspase-3 (active p17 and inactive p20) levels were determined by immunoblotting. **c,** Upregulation of myogenin and formation of caspase-3 p17 were evaluated in the presence of 0, 25, or 100 ng/mL FK506 by immunoblotting. **d,** A working model for caspase activation, peripheral Nup degradation, and myogenin upregulation during myoblast-to-myotube conversion. **e**, C2C12 cells that have undergone myogenic differentiation for 1 day were immunostained for myogenin, Nup153, and Tpr. In yellow and blue dashed boxes are myogenin-negative and -positive $TprC^{-}$ cells, respectively.

Figure 5 | Caspase-mediated NPC trimming occurs during neurogenesis and ER stress. a, Expression levels of caspase-inhibiting proteins (cIAP-1/2, XIAP, survivin), neuronal differentiation markers (Sox2 and βIII-tubulin), caspase substrates (Nup153 and PARP), and active caspase-3 (p17) in differentiating neurons were determined by western blotting. **b,** Acute ER stress was induced using 1 μg/mL tunicamycin in C2C12 myotubes, reserve cells, and myoblasts, and the levels of Nups, BiP, caspase-inhibiting proteins (cIAP-1/2 and XIAP), myosin heavy chain (MHC), myogenin, and active caspase-3 (p17) were monitored by immunoblotting. **c,** Chronic ER stress was induced in differentiated C2C12 cells for 7 days using low doses of tunicamycin (0, 10, 25, or 50 ng/mL). The integrity of Nups and the induction of BiP and active caspase-3 (p17) were assessed by immunoblotting. **d,** Schematic representation illustrating caspase activation and NPC proteolysis patterns in apoptosis, cell differentiation, and ER stress.

Methods

Antibodies and chemicals. Primary and secondary antibodies and chemicals used in this study are summarized in **Supplementary Table 2, 3, and 4**.

Immunoblot techniques. Cultured cells were washed with phosphate-buffered saline (PBS) and harvested by trypsinization. Cell pellet was washed with PBS, and lysed in RIPA buffer (50 mM Tris-HCl pH 7.5, 150 mM NaCl, 1% Triton X100, 0.5% sodium deoxycholate, 0.1% sodium dodecyl sulfate) containing protease and phosphatase inhibitors (Pierce Protease Inhibitor Mini Tablet, EDTA-free, Thermo Scientific; PhosSTOP, Roche) for 45 minutes at 4ºC. Insoluble material was pelleted at 16,000 x g at 4ºC for 20 minutes. 15-30 μg of total protein per sample were added 6x Laemmli sample buffer, boiled for 4 minutes, and loaded on a Tris or Bis-tris gel for electrophoresis. Proteins were transferred to a nitrocellulose membrane and stained with Ponceau S solution to confirm equal protein loading and successful transfer. After washing with Tris-buffered saline containing 0.05% (w/v) Tween 20 (TBST) several times, the membrane was blocked with 5% non-fat milk power in TBST for an hour at room temperature, and subsequently immunoblotted at 4ºC overnight with primary antibodies listed in **Supplementary Table 2**. Chemiluminescent detection was conducted using either SuperSignal West Pico or Femto kits (Thermo Scientific) after 45-minute incubation with secondary antibodies listed in **Supplementary Table 3** at room temperature. Western blot images were obtained using KwikQuant Imager (Kindle Biosciences) or Odyssey CLx (LI-COR).

Cloning. Vectors, PCR templates, and PCR primers used in this study are listed in **Supplementary Table 5**. In-fusion cloning was performed using the In-Fusion HD EcoDry Cloning Plus kit (Takara), and standard cut-and-paste cloning using T7 DNA ligase (New England Biolabs).

Cell culture. C2C12 and HCT116 cells were obtained from ATCC. C2C12 cells were cultured in Dulbecco's Modified Eagle Medium (DMEM) supplemented with 20% fetal bovine serum and penicillin-streptomycin. For myogenic differentiation, they were grown to confluency, washed with PBS twice, and added DMEM with 2% horse serum and the same antibiotics. C2C12 differentiation medium was replenished every 24 or 48 hours. After 120 hours, mature myotubes and reserve cells were obtained. Myotubes were harvested with minimal contamination of reserve cells by mild trypsinization (1:3 or 1:4 dilution of trypsin in PBS). HCT116 cells were cultured in

McCoy's 5A Medium supplemented with 10% fetal bovine serum and penicillin-streptomycin. H9 embryonic stem cells were differentiated to neural precursor cells using a previously published method[45]. Purified neural precursor cells were cultured in neurogenic conditions (DMEM/F12 based medium with 1x N2, 1x B27, 20ng/mL GDNF, 20ng/mL BDNF, 1mM cAMP, and 200nM ascorbic acid) for 4 weeks to generate mature post-mitotic neurons.

C2C12 cell fractionation. Cells were harvested by trypsinization, washed with PBS, and chilled on ice. Cells were then lysed in ice-cold 0.1% NP40 in PBS, and rotated at 4ºC for 10 minutes. Nuclei were pelleted by centrifugation at 500 x g at 4ºC for 4 minutes, and the supernatant (cytoplasmic fraction) was transferred to a fresh tube and stored at -80ºC until use. Nuclei were again resuspended in ice-cold 0.1% NP40 in PBS, rotated at 4ºC for 5 minutes, and pelleted at 500 x g at 4ºC for 4 minutes. The supernatant was discarded, and the pellet (nuclear fraction) was stored at -80ºC until use.

Lentivirus packaging, infection, and selection. Third-generation lentiviral protocol was followed to produced virus in HEK293T cells (obtained from the Salk Stem Cell Core Facility). C2C12 cells were infected with viral supernatant at 30-40% confluency in the presence of 6 μg/mL polybrene for 24 hours, and selected 24 hours after infection with 1 mg/mL puromycin.

RNA fluorescence *in situ* hybridization (FISH). C2C12 cells were grown on a No. 1.5 coverslip placed in a 12-well cell culture plate. After removing media, cells were washed with PBS, and fixed in 3.7% paraformaldehyde in PBS for 10 minutes at room temperature. Fixed cells were washed with PBS twice and permeabilized in 70% (vol/vol) ethanol at 4ºC for at least a day. We then followed Stellaris RNA FISH protocol for adherent cells (https://www.biosearchtech.com/support/resources/stellaris-protocols) to fluorescently visualize RNAs. Fluorescent images were obtained using a Leica SP8 confocal microscope equipped with a 63x oil-immersion objective. Images were cropped and pseudocolored using FIJI. See **Supplementary Table 6** for RNA FISH probes used in this study.

Immunofluorescence. C2C12 cells and mouse primary myoblasts were grown on a chambered cell culture slide (Ibidi). For the latter, slides were coated with Matrigel prior to seeding. Cells were fixed in PBS containing 2% paraformaldehyde for 10 minutes at room temperature, and washed with PBS 3 times. Fixed cells were permeabilized and blocked in immunofluorescence buffer (PBS containing 0.1% Triton-X, 0.02% sodium dodecyl sulfate, and 10 mg/mL bovine serum

albumin) for 30 minutes. The cells were then incubated with primary antibodies diluted in immunofluorescence buffer at room temperature for 2 hours, washed 3 times with immunofluorescence buffer, and incubated with the appropriate secondary antibodies diluted in immunofluorescence buffer at room temperature for 45 minutes. Finally, the cells were washed with immunofluorescence buffer 3 times, and added VECTASHIELD antifade mounting medium with DAPI (Vector Laboratories). Fluorescent images were obtained using a Leica SP8 confocal microscope equipped with a 63x oil-immersion objective. Images were cropped and pseudocolored using FIJI. See **Supplementary Table 2 and 3** for antibodies used for immunofluorescence.

Poly(A)$^+$ RNA quantification. Poly(A)$^+$ RNA was isolated from nuclei and whole cells (see C2C12 cell fractionation above) using the Magnetic mRNA Isolation Kit (New England Biolabs). Two rounds of binding, washing, and elution were performed. Eluted RNA was quantified via Qubit RNA HS Assay (Invitrogen).

Dextran exclusion assay. 20, 40, and 65-85 kDa dextrans (Sigma, FD20S/FD40S/T1162) were dissolved in "Transport Buffer (TB)" (20 mM HEPES (pH 7.3), 110 mM potassium acetate, 5 mM sodium acetate, 1 mM EGTA, and 2 mM DTT) at 10 mg/ml. Degradation products were removed using 10 and 30 kDa-cutoff size exclusion columns (Millipore UFC501096/UFC503096). Dextran stock solutions were diluted in TB 1:50 to 1:200 prior to use. C2C12 cells seeded in a chambered cell culture slides were incubated with TB supplemented with 20 μg/ml digitonin for 5 min at room temperature, washed with TB (without digitonin) three times, and added dextrans. After 7.5 min at 37ºC, images were acquired using a Leica SP8 confocal microscope equipped with a 63x oil-immersion objective. Images were cropped and pseudocolored using FIJI.

MBD2 CUT&RUN-sequencing. 300-400 thousand cells were used for each CUT&RUN-sequencing reaction. C2C12 cells were harvested by trypsinization, washed in PBS, and stored in fetal bovine serum supplemented with 10% dimethyl sulfoxide until use. MBD2-bound genomic fragments were prepared using the CUT&RUN assay kit (Cell Signaling Technology, 86652). MBD2 antibody (Sigma, M7318) was used at 10 μg/mL. Sequencing libraries were prepared using NEBNext Ultra II DNA library prep kit for Illumina and NEBNext Multiplex Oligos for Illumina (New England Biolabs, E7645 and E7600). Libraries were quantified and analyzed using Qubit dsDNA HS assay kit (Thermo Fisher Scientific) and a TapeStation 2200 with high-sensitivity DNA kit (Agilent). Libraries were sequenced in paired-end 150 base pair mode on the Illumina NovaSeq

6000 platform. Paired-end fragments were trimmed, mapped to the mm10 genome, and filtered using Trim Galore (https://github.com/FelixKrueger/TrimGalore), Bowtie2[46], and SAMtools[47], respectively. Peaks were identified using MACS2[48] and further filtered and analyzed with in-house Python scripts that leveraged pyBigWig (https://github.com/deeptools/pyBigWig) and pyBedTools[49] packages. GO term analyses (biological processes) were performed on http://metascape.org[50]. Genomic annotation of the peaks was conducted using ChIPseeker[51]. CUT&RUN-sequencing data were plotted using karyoploteR[52].

mRNA-sequencing. 1-2 million C2C12 cells were lysed in 1 ml TRIzol. 0.4 ml chloroform was added and vigorously shaken for RNA extraction. The aqueous phase was transferred to a fresh tube, and one volume of 70% ethanol was added dropwise while vortexing at the lowest speed at room temperature. The mixture was purified using RNeasy Mini kit (Qiagen) to yield several hundred ng/μL total RNA. mRNA-sequencing was performed in paired-end 150 base pair mode on the Illumina NovaSeq 6000 platform. Paired-end fragments were mapped to mm10, filtered, and assembled into transcripts using HISAT2[53], SAMtools[47], and StringTie[54]. Differential expression was evaluated using DESeq2[55], and further analyzed with in-house python scripts.

References

45 Marchetto, M. C. *et al.* Altered proliferation and networks in neural cells derived from idiopathic autistic individuals. *Mol Psychiatry* **22**, 820-835 (2017).

46 Langmead, B. & Salzberg, S. L. Fast gapped-read alignment with Bowtie 2. *Nat Methods* **9**, 357-359 (2012).

47 Li, H. *et al.* The Sequence Alignment/Map format and SAMtools. *Bioinformatics* **25**, 2078-2079 (2009).

48 Zhang, Y. *et al.* Model-based analysis of ChIP-Seq (MACS). *Genome Biol* **9**, R137 (2008).

49 Dale, R. K., Pedersen, B. S. & Quinlan, A. R. Pybedtools: a flexible Python library for manipulating genomic datasets and annotations. *Bioinformatics* **27**, 3423-3424 (2011).

50 Zhou, Y. *et al.* Metascape provides a biologist-oriented resource for the analysis of systems-level datasets. *Nat Commun* **10**, 1523 (2019).

51 Yu, G., Wang, L. G. & He, Q. Y. ChIPseeker: an R/Bioconductor package for ChIP peak annotation, comparison and visualization. *Bioinformatics* **31**, 2382-2383 (2015).

52 Gel, B. & Serra, E. karyoploteR: an R/Bioconductor package to plot customizable genomes displaying arbitrary data. *Bioinformatics* **33**, 3088-3090 (2017).

53 Kim, D., Paggi, J. M., Park, C., Bennett, C. & Salzberg, S. L. Graph-based genome alignment and genotyping with HISAT2 and HISAT-genotype. *Nat Biotechnol* **37**, 907-915 (2019).

54 Pertea, M. *et al.* StringTie enables improved reconstruction of a transcriptome from RNA-seq reads. *Nat Biotechnol* **33**, 290-295 (2015).

55 Love, M. I., Huber, W. & Anders, S. Moderated estimation of fold change and dispersion for RNA-seq data with DESeq2. *Genome Biol* **15**, 550 (2014).